Journal of
Synchrotron
Radiation

ISSN 1600-5775

Received 7 March 2013
Accepted 30 August 2013

Integration method for directly analyzing interface statistics of periodic multilayers from X-ray scattering

Haochuan Li,[a] Jingtao Zhu,[a]* Zhanshan Wang,[a] Hong Chen,[a] Yuzhu Wang[b] and Jie Wang[b]

[a]MOE Key Laboratory of Advanced Micro-structured Materials, Institute of Precision Optical Engineering, Department of Physics, Tongji University, Shanghai 200092, People's Republic of China, and [b]Shanghai Synchrotron Radiation Facility, Shanghai Institute of Applied Physics, Chinese Academy of Sciences, Shanghai 201204, People's Republic of China. *E-mail: jtzhu@tongji.edu.cn

An integration method is demonstrated for directly determining the average interface statistics of periodic multilayers from the X-ray scattering diagram. By measuring the X-ray scattering diagram in the out-of-plane geometry and integrating the scattered intensity along the vertical momentum transfer q_z in an interval, which is decided by the thickness ratio Γ (ratio of sublayer's thickness to periodic thickness), the cross-correlations between different interfaces are canceled and only the autocorrelations are reserved. Then the multilayer can be treated as a 'single interface' and the average power spectral density can be obtained without assuming any vertical correlation model. This method has been employed to study the interface morphology of sputter-deposited W/Si multilayers grown at an Ar pressure of 1–7 mTorr. The results show an increase in vertical correlation length and a decrease in lateral correlation length with increased Ar pressure. The static roughness exponent $\alpha = 0$ and dynamic growth exponent $z = 2$ indicate the Edwards–Wilkinson growth model at an Ar pressure of 1–5 mTorr. At an Ar pressure of 7 mTorr, $\alpha = 0.35$ and $z = 1.65$ indicate the Kardar–Parisi–Zhang growth model.

Keywords: X-ray scattering; multilayer; interface morphology; power spectral density; dynamic scaling.

1. Introduction

X-ray diffuse scattering has become an invaluable tool for investigating buried interfaces in nanometer thin films with the advantage of high sensitivity to lateral structures, simplicity of non-destructive measurement, high spatial frequency, and the possibility of *in situ* experiments (Gibaud & Hazra, 2000; Müller-Buschbaum, 2003; Renaud *et al.*, 2009). The main issue when using X-ray scattering methods is to extract statistical properties of the interfaces from a measured scattering diagram. Although theoretical studies (Sinha *et al.*, 1988; Stearns, 1992; Holý & Baumbach, 1994; de Boer, 1996) have shown that the scattered intensity is determined by the autocorrelation and cross-correlation functions of the interfaces, the inverse problem is rather intractable. Up to now the most general method used in X-ray scattering data analysis of multilayers is model-based parameter fitting. The fitting method is, however, very ambiguous and tedious. Thus finding a direct method without ambiguousness is expected to give more reliable results.

It has been shown (Kozhevnikov & Pyatakhin, 2000) that the scattered intensity of a single interface is proportional to the power spectral density (PSD), which is the Fourier transformation of the autocorrelation function. This fact allows us to unambiguously determine the statistics of a single interface from X-ray scattering measurements. For thin films with more than one interface, the cross-correlations between different interfaces occur in the scattered intensity. A method was demonstrated (Peverini *et al.*, 2007) to directly determine the PSDs of both interfaces for monolayer thin films by measuring both scattering diagrams before and after thin film deposition. This method utilizes the properties that the coefficient of the cross-correlation term (there is only one cross-correlation term for a monolayer) equals zero at specific spatial frequencies and that the PSD is a smooth function of the spatial frequency. However, this method cannot be applied to multilayers which have more than two interfaces because different cross-correlation terms have different zero points.

Salditt *et al.* (1994, 1995, 1996) proposed an integration method for directly analyzing the X-ray scattering diagram of

periodic multilayers. The integration method involves integrating the scattered intensities along the vertical momentum transfer q_z over one 'Brillouin zone', *i.e.* from $(2m-1)\pi/\Lambda$ to $(2m+1)\pi/\Lambda$, where m is a positive integer and Λ is the multilayer period. Then the cross-correlations between different interfaces are expected to cancel and only the autocorrelations are reserved. Then the multilayer can be treated as a 'single interface' and an average PSD can be obtained.

The integration method was introduced without proof or derivation by Salditt and followed by several other studies (Spizzo *et al.*, 2009; Siffalovic *et al.*, 2010*a*,*b*). In this work we reviewed the integration method and surprisingly found that it is not generally correct though its basic idea is inspiring. Salditt's original integration method can only cancel the cross-correlations between interfaces with the same type. Here the type of interface in a periodic A/B multilayer refers to whether it is A-on-B or B-on-A. Then we revised the integration method to be able to cancel all the cross-correlations. In our revised version the integration interval must be chosen according to the thickness ratio Γ (ratio of sublayer's thickness to periodic thickness). The theoretical derivation and discussion are presented in §2. Then we apply the integration method to investigate the effect of Ar pressure on the interface morphology of sputter-deposited W/Si multilayers in §3. In §4 we give a summary of this work and our conclusion.

2. Theory of the integration method

2.1. Theoretical background for X-ray scattering

Fig. 1(*a*) shows a schematic illustration of the scattering geometry. Letting the average sample surface be the xy plane and the incident plane be the xz plane, a rough interface can then be described by the height deviation from its average position $h(r)$, $r \equiv (x, y)$. The height–height correlation functions are defined as $C_{i,j}(R) = \langle h_i(r)h_j(r+R)\rangle_r$, where $\langle\ldots\rangle_r$ denotes the assemble average of r and R is the lateral distance of two positions. Autocorrelations are described if $i = j$ while cross-correlations between different interfaces if $i \neq j$. If $\mathbf{q} = \mathbf{k}_s - \mathbf{k}_i$ ($\mathbf{k}_i$ and $\mathbf{k}_s$ are the incident and scattered wavevector, respectively) denotes the momentum transfer, the diffuse scattering is measured with a non-zero parallel momentum transfer $q_\parallel = (q_x^2 + q_y^2)^{1/2}$. When the grazing incident angle θ_0, grazing scattering angle θ and the azimuth scattering angle φ are small, $q_x \simeq k_0(\theta_0^2 - \theta^2 - \varphi^2)/2$, $q_y \simeq k_0\varphi$ and $q_z \simeq k_0(\theta_0 + \theta)$ where k_0 is the wavenumber in a vacuum. In the out-of-plane geometry ($\varphi = 0$), $|q_y| \gg |q_x|$ gives $q_\parallel \simeq q_y$. In the in-plane geometry ($\varphi \neq 0$), $q_\parallel = q_x$ as $q_y = 0$. Thus the maximum accessible spatial frequency in the out-of-plane geometry is much larger than in the in-plane geometry. Another advantage of the out-of-plane geometry is that the lateral and vertical components of the momentum transfer are independent of each other and thus sufficiently validate the usage of the simpler kinetic Born approximation (BA) theory provided that $\theta_0, \theta > \theta_c$ where θ_c denotes the critical angle for total external reflection (TER). In BA theory, the scattered intensity is calculated as (Sinha, 1994)

$$I_{\rm DIFF}^{\rm BA} \propto \sum_{i,j} \Delta\varepsilon_i \Delta\varepsilon_j^* \exp\left[-iq_z\left(z_i - z_j\right)\right] q_z^{-2} \times \exp\left[-q_z^2\left(\sigma_i^2 + \sigma_j^2\right)/2\right] \times \int \exp\left[q_z^2 C_{i,j}(R)\right] \exp\left(-iq_\parallel R\right) {\rm d}^2R, \quad (1)$$

where $\Delta\varepsilon_i$ is the change in permittivity across the ith interface, z_i is the average position of the ith interface, and σ_i is the roughness of the ith interface. Considering the periodic A/B multilayer illustrated in Fig. 1(*b*), let N be the periodic number, Λ the periodic thickness, and Γ the thickness ratio [the thicknesses of A and B are then $\Lambda_A = \Gamma\Lambda$ and $\Lambda_B = (1-\Gamma)\Lambda$]. There are two types of interfaces in this multilayer, B-on-A and A-on-B, and they are indexed as $i = 2u$ and $i = 2u-1$, respectively (u is an integer and $1 \leq u \leq N$). Then we can obtain $z_{i=2u} = u\Lambda$, $z_{i=2u-1} = (u-\Gamma)\Lambda$, and $\Delta\varepsilon_i = (-1)^i\Delta\varepsilon$ ($\Delta\varepsilon = \varepsilon_A - \varepsilon_B$ is the difference in permittivity of the two materials). If the roughness is small [$|q_z^2 C(R)| \ll 1$], which is usually matched at grazing angles in the interested high-frequency range, the exponential terms in the integration in equation (1) can be expanded. After adding equation (1) to itself and pairing the i,j terms with j,i terms, equation (1) is simplified to

$$I_{\rm DIFF}^{\rm BA} \propto \sum_{i,j} (-1)^{i+j} \exp\left[-q_z^2\left(\sigma_i^2 + \sigma_j^2\right)/2\right] \times \cos\left[q_z\left(z_i - z_j\right)\right] F_{i,j}, \quad (2)$$

where $F_{i,j} = (2\pi)^{-2}\int C_{i,j}(R)\exp(iqr)\,{\rm d}^2R$ is the Fourier transformation of the correlation function and the PSD function is then defined as ${\rm PSD}_i = F_{i,i}$. In equation (2) we can see that at positions $q_z = n2\pi/\Lambda$ the cross-correlations between interfaces with distance of $m\Lambda$ will add in phase (m and n are positive integers). This property gives rise to the so-called Bragg sheet or diffuse Bragg-like peak. Multiplying (2) by $\exp(q_z^2\sigma_{\rm av}^2)$, where $\sigma_{\rm av}$ is the average value of roughnesses for all the interfaces in the multilayer, we can further cancel the exponential term in (2) provided that the roughnesses of different interfaces do not differ too much. The average roughness can be prior obtained by X-ray reflectometry.

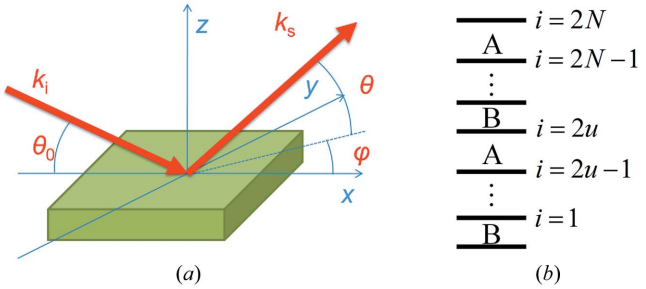

Figure 1
Illustration of (*a*) the scattering geometry and (*b*) the multilayer structure.

2.2. Integrating scattered intensity along q_z

The essence of the integration method is integrating the scattered intensity along q_z and thus eliminating the cross-

correlation terms with $i \neq j$ considering the periodicity of the cosine term in equation (2). After multiplying the average roughness term $\exp(q_z^2\sigma_{\rm av}^2)$ and integrating the production over an interval with center at q_0 and width of Δq, we obtain the integrated intensity,

$$I_{\rm INT} = \int_{q_0-\Delta q/2}^{q_0+\Delta q/2} I_{\rm DIFF}^{\rm BA} \exp\left(q_z^2\sigma_{\rm av}^2\right) {\rm d}q_z \propto \sum_{i,j} (-1)^{i+j} F_{i,j} \int_{q_0-\Delta q/2}^{q_0+\Delta q/2} \cos\left[q_z\left(z_i - z_j\right)\right] {\rm d}q_z. \quad (3)$$

The terms in (3) can be classified into three types according to the configuration of i and j.

2.2.1. Autocorrelations. The $i = j$ terms represent the autocorrelation of the interfaces. Substituting $z_i - z_j = 0$, we obtain the integrated intensity,

$$I_{\rm INT}^{\rm (I)} = \Delta q \sum {\rm PSD}_i. \quad (4a)$$

The autocorrelation of each interface is reserved in the integrated intensity.

2.2.2. Cross-correlations between interfaces with the same type. The $i \neq j$ and $i - j = 2k$ (k is an integer) terms represent the cross-correlation between two interfaces with the same type, *i.e.* the two interfaces are either both A-on-B or both B-on-A. In this case, $z_i - z_j = k\Lambda$ and

$$I_{\rm INT}^{\rm (II)} = (2/\Lambda) \sum_{i-j=2k} F_{i,j} (1/k) \cos(k\Lambda q_0) \sin(k\Lambda\Delta q/2). \quad (4b)$$

The zero points of equation (4*b*) are $\Delta q = l2\pi/\Lambda$ (l is a positive integer). Using any integration interval of this width can cancel the cross-correlation terms between interfaces with the same type. This part agrees with the idea of Salditt.

2.2.3. Cross-correlations between interfaces with different types. The $i \neq j$ and $i - j = 2k + 1$ (k is an integer) terms represent the cross-correlation between two interfaces with different types, *i.e.* one interface is A-on-B and the other is B-on-A. Recall the pairing of the i,j term and j,i term in equation (1) to derive equation (2). Thus the i,j term and j,i term are identical since equation (2) and we only consider the $i = 2u$ and $j = 2v - 1$ case ($u - v = k$, u, v are integers and $1 \leq u, v \leq N$). In this case, $z_i - z_j = (k + \Gamma)\Lambda$ and

$$I_{\rm INT}^{\rm (III)} = -(4/\Lambda) \sum_{i-j=2k+1} F_{i,j} \frac{(-1)^{kl}}{k+\Gamma} \times \cos\left[(k+\Gamma)\Lambda q_0\right] \sin(l\,\Gamma\pi). \quad (4c)$$

There are two conditions for Γ that either one will make equation (4*c*) equal to zero for any k. They are

$$\Gamma = \left(2n^{(1)} + 1\right)/2m \quad (5a)$$

and

$$\Gamma = n^{(2)}/l \quad (5b)$$

[$n^{(1)}$, $n^{(2)}$ and m are integers]. When equation (5*a*) is used, an additional restriction, $q_0 = m\pi/\Gamma$, must be adopted. Choosing the smallest $l = 1$, the integration interval is then $([m-1]\pi/\Lambda, [m+1]\pi/\Lambda)$ (m must be no less than 2 to avoid the TER region). When equation (5*b*) is used, the integration interval can be chosen to be $(\pi/\Lambda, [2l+1]\pi/\Lambda)$ considering the minimal but away from the TER region. Apparently any Γ derived from (5*a*) can match (5*b*) and the integration interval using (5*a*) is smaller than that using (5*b*), which is an advantage for experimental realisation. Thus (5*b*) shall be used only when (5*a*) fails.

To quantitatively compare the cross-correlation terms with the autocorrelation terms when Γ and the integration interval do not satisfy the above conditions, we have to make some assumptions which are not necessary for the integration method. The first assumption is about the cross-correlation. We introduce a commonly used cross-correlation model $F_{i,j} = ({\rm PSD}_i\,{\rm PSD}_j)^{1/2} \exp(-|z_i - z_j|/\xi_\perp)$, where $\xi_\perp$ is the characteristic vertical correlation length. The second assumption is that all the interfaces with the same types have the same PSD, *i.e.* all the B-on-A (A-on-B) interfaces have the same ${\rm PSD}_{A(B)}$. Then we carry on calculating equations (4*a*) and (4*c*) with $\Delta q = 2l\pi/\Lambda$ and $q_0 = m\pi/\Lambda$. After some mathematics we obtain the integrated intensity,

$$I_{\rm INT}^{\rm (I)} = \frac{2N\pi}{\Lambda} \frac{{\rm PSD}_A + {\rm PSD}_B}{2} \quad (6a)$$

and

$$I_{\rm INT}^{\rm (III)} = -(4N/\Lambda)\cos(m\Gamma\pi)\cos(l\,\Gamma\pi) \times \sum_{k=1-N}^{k=N-1} \frac{1-|k|/N}{k+\Gamma}(-1)^{k(m+l)} \times \exp(-|k+\Gamma|\Lambda/\xi_\perp)({\rm PSD}_A\,{\rm PSD}_B)^{1/2}. \quad (6b)$$

Considering an extreme situation where the vertical correlation is very weak and only the cross-correlations between adjacent layers are finite, we calculate the absolute value of the coefficients in (6*a*) and (6*b*) *versus* Γ with $\xi_\perp = \Lambda$ and $k = 0, -1$. The results for different m ($l = 1$) are shown in Fig. 2. Only values in the $0 < \Gamma \leq 1/2$ region are plotted considering the symmetry between Γ and $1 - \Gamma$. As can be seen, the integrated cross-correlations between interfaces with different types (solid lines with symbols) are comparable with the autocorrelation terms (dashed line) even in very weak vertical correlation when Γ does not match (5*a*) or (5*b*). These cross-correlation terms are underestimated by Salditt and are not negligible. To cancel all cross-correlations we must choose the integration interval according to Γ. The value of Γ can be deduced by using calibrated deposition rate and deposition time or from the fitting of specular reflectance.

2.3. Summary of the integration method

As a summary of §2, we have revised the integration method which can directly determine the average PSD function of a periodic multilayer from the X-ray scattering diagram measured in the out-of-plane geometry. By integrating an interval along q_z, the cross-correlation terms in the integrated intensity cancel and only the autocorrelation terms are reserved. The validity of this method depends on the thickness ratio Γ and carefully choosing the integration interval

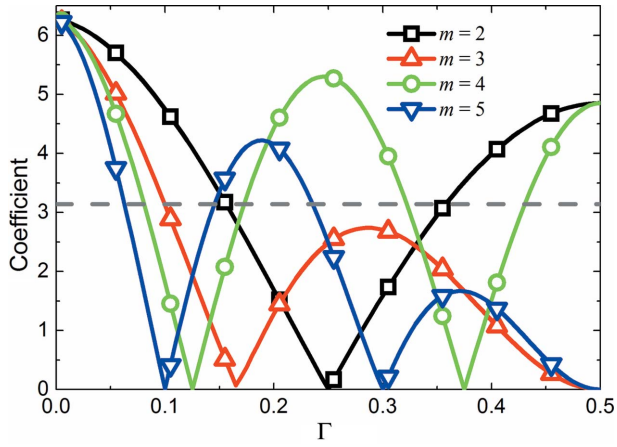

Figure 2
Absolute value of the coefficients in the integrated intensity *versus* thickness ratio. The dashed line is for the autocorrelation terms. Solid lines are for the cross-correlation terms with different integration intervals $([m-1]\pi/\Lambda, [m+1]\pi/\Lambda)$.

according to Γ. Theoretically any Γ with a rational value r/s (r and s are integers) is valid with the integration interval $(\pi/\Lambda, [2s+1]\pi/\Lambda)$. If Γ further matches the condition that r is an odd integer and s is a larger-than-2 even integer, a more practical integration interval $([s-1]\pi/\Lambda, [s+1]\pi/\Lambda)$ can be applied. However, the accessible range of q_z in real experiments is limited. We plot the values of Γ that can be used when $q_z \leq 9\pi/\Lambda$, which means that the first four Bragg sheets can be observed in experiments, in Fig. 3. Only values in the $0 < \Gamma \leq 1/2$ region are plotted considering the symmetry between Γ and $1-\Gamma$. The vertical position of the thick solid lines in the figure denotes the corresponding integration interval. If more than one interval is applicable for a single Γ value, the interval with a smaller upper-bond is chosen. As can be seen from the figure, a variety of Γ are available for experimental realisation. If some error of about 0.02 in Γ is tolerated, a multilayer with almost any Γ can be analyzed with the integration method.

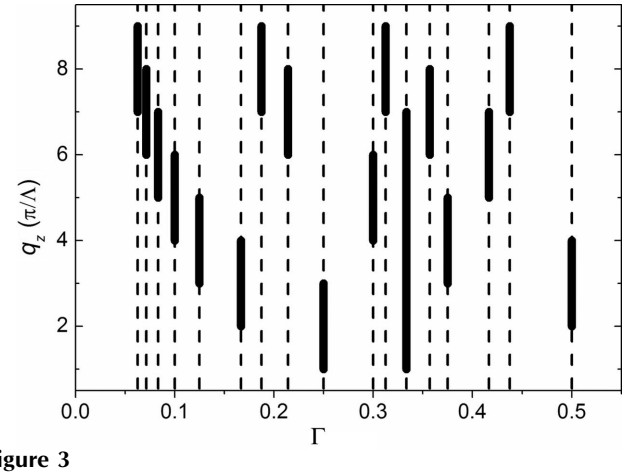

Figure 3
Available thickness ratio when q_z is not larger than $9\pi/\Lambda$. The vertical position of the thick lines denotes the corresponding integration interval.

3. Experimental application on W/Si multilayers

In this section, we present the successful application of the integration method on characterizing the interface morphology of sputter-deposited W/Si multilayers grown at different Ar pressure. The W/Si multilayers are important reflectors for both soft and hard X-rays.

3.1. Experimental details and results

The W/Si multilayers were deposited onto polished silicon (100) wafers with surface roughness of about 0.3 nm by an ultrahigh-vacuum direct-current magnetron sputtering system. The pressure before all depositions was below 3.7×10^{-7} Torr. Four samples were deposited at Ar pressures of 1, 3, 5 and 7 mTorr (designated as S-1, S-2, S-3 and S-4, respectively) with identical bilayer number $N = 10$ and similar period thickness $\Lambda \simeq 7.5$ nm. The thickness ratio was chosen to be $\Gamma = 1/4$ (W layer thickness $\Lambda_W \simeq 1.9$ nm), and thus gives the integration interval of $(\pi/\Lambda, 3\pi/\Lambda)$.

After deposition, the multilayers were characterized by low-angle X-ray reflectometry (XRR). The measurements were made on a four-circle X-ray diffractometer with a Cu sealed-tube source and a Si (220) crystal monochromator tuned to the Cu $K\alpha$ line ($\lambda = 0.154$ nm). The results are shown in Fig. 4 (plotted as thick black lines). The first seven Bragg peaks can be distinctly observed for S-1, S-2 and S-3 while only five peaks for S-4, indicating a much larger roughness for S-4. All four XRR curves have a vanished fourth-order peak due to $\Gamma = 1/4$. All the curves were fitted in the Bede *REFS* program which uses the well known recursive formula (Underwood & Barbee Jr, 1981) for calculating the reflectivity and differential

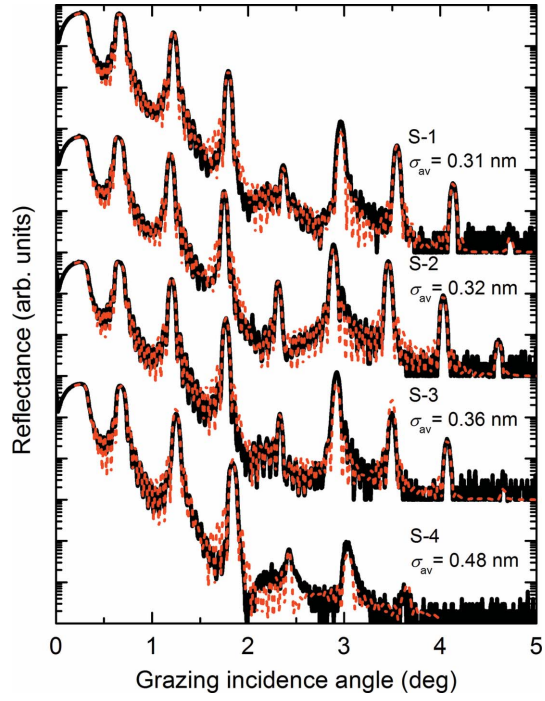

Figure 4
Measured (black solid lines) and fitted (red dashed lines) low-angle X-ray reflection curves of the four W/Si samples.

evolution algorithm (Wormington *et al.*, 1999) for parameter optimization. The fitted curves (plotted as thin red lines) are in good agreement with the measured ones. The four fitted Λ values are in the range 7.3–7.5 nm and Γ in the range 0.25–0.27. The averaged roughness is 0.31, 0.32, 0.36 and 0.48 nm for S-1, S-2, S-3 and S-4, respectively.

The scattering measurements were made at beamline BL16B1 of the Shanghai Synchrotron Radiation Facility. X-rays were provided from a bending magnet and tuned to 10 keV (λ = 0.124 nm) by a Si (111) double-crystal monochromator with an energy resolution of about 6×10^{-4}. High-order harmonics were suppressed by the total external reflection cut-off of the focusing mirror. The light spot size at the sample stage was about 0.5 mm × 0.5 mm. The scattered X-rays were recorded by a circular CCD detector with a diameter of 170 mm (2048 pixels), 2.1 m downstream from the sample stage. A vacuum tube was mounted between the sample stage and detector to minimize absorption and a beamstop was inserted to shade the reflected beam. In the small grazing incident/scattering angle range, this experimental set-up directly measures the scattering diagram in the $q_z q_y$ plane. The scattering diagrams measured at grazing incident angle $\theta_0 = 0.37^\circ$ for the four W/Si samples are shown in Fig. 5. The first two Bragg sheets were observed in all four samples. Between the Bragg sheets, the scattered intensity is also modulated along q_z at low q_y. This effect is analog to the Kiessig fringes and implies that the interfaces are correlated to a large extent at low frequencies. S-1 and S-2 have similar scattering diagrams. S-3 has longer (in the q_y direction) Bragg sheets and S-4 the longest.

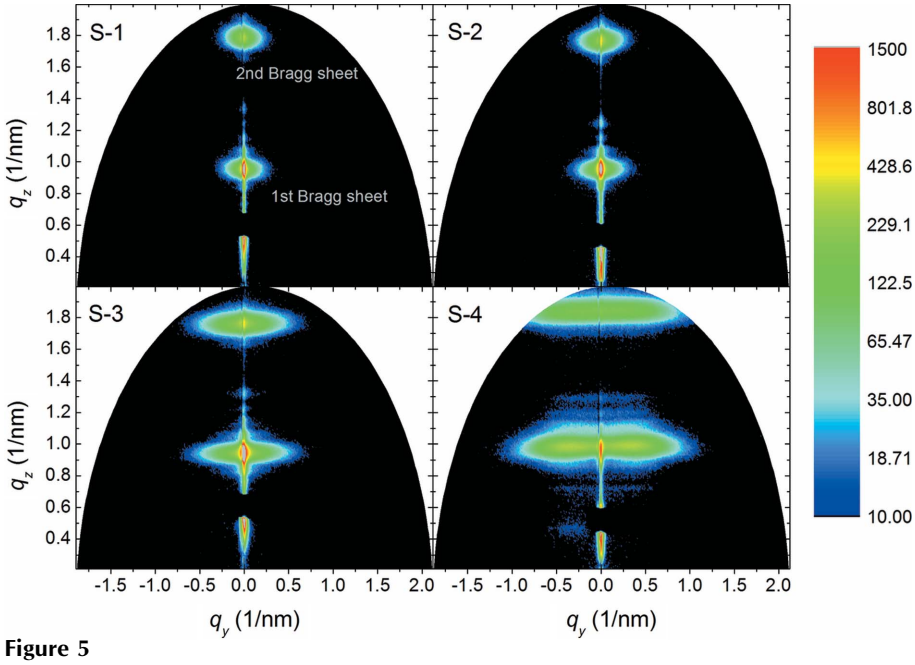

Figure 5
Measured X-ray scattering diagrams of the four W/Si samples.

3.2. Analyses and discussion

Now we apply the integration method to analyze the measured diagrams. The scattered intensity is multiplied by the average roughness term $\exp(q_z^2\sigma_{\rm av}^2)$ and integrated along q_z in the $(\pi/\Lambda, 3\pi/\Lambda)$ interval as Γ = 1/4. The integrated intensity is proportional to the average PSD function which is the Fourier transformation of the autocorrelation function. The most general model for autocorrelation is the isotropic self-affine model (Sinha *et al.*, 1988) with $C(R) = \sigma^2 \exp[-(R/\xi_\parallel)^{2\alpha}]$, where σ is the root mean square (r.m.s.) roughness, $\xi_\parallel$ the characteristic lateral correlation length, and α the static roughness exponent (also called the fractal exponent) with the value $0 < \alpha \leq 1$. For $R \gg \xi_\parallel$, $C(R) \to 0$. For $R \ll \xi_\parallel$, an asymptotic behavior $C(R) \simeq A - BR^{2\alpha}$ (A and B are constants) is presented. Thus the PSD function follows the asymptotic behavior PSD $\propto q_\parallel^{-\gamma}$ at high frequencies $q_\parallel \gg 2\pi/\xi_\parallel$ with the exponent $\gamma = 2 + 2\alpha$. Other autocorrelation models also feature this basic asymptotic behavior as it is generally observed and predicted within the theory of kinetic roughening (Barabási & Stanley, 1995; Krug, 1997).

The deduced PSDs of the four samples are shown in Fig. 6 as open symbols. The profiles of S-1, S-2 and S-3 are similar. They all show a linear feature in the log–log plot at high q_y values, thus confirming the power-law asymptotic behavior. The exponent γ was found to be 1.95, 1.97 and 2.03 for S-1, S-2 and S-3 by power-law fit. The exponents are approximately associated with $\alpha \simeq 0$. The behavior of S-4 is quite different from the others at low q_y, but the power-law asymptotic behavior is also observed at high q_y with the exponent γ = 2.70. This exponent is associated with α = 0.35. The difference in the roughness exponent α reveals different growth mode. Another significant statistic, lateral correlation length $\xi_\parallel$, can be obtained from the integrated intensity. Considering the different asymptotic behavior between $R \gg \xi_\parallel$ and $R \ll \xi_\parallel$, the

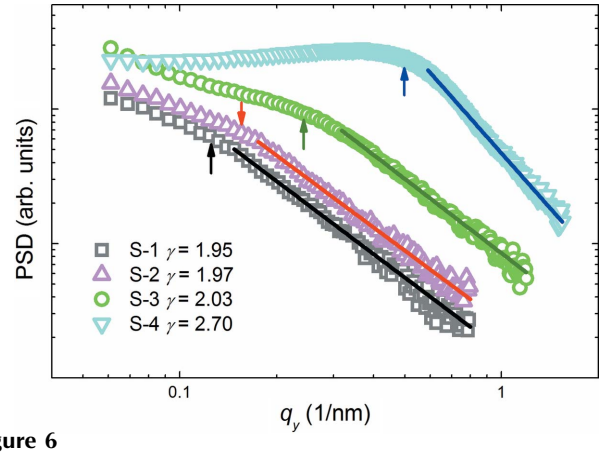

Figure 6
PSDs (open symbols) of the four W/Si samples *versus* q_y. Solid lines are the power-law fit. Arrows denote the critical point for the change of slope.

change of slope in Fig. 6 gives a measure of $\xi_{\parallel}$. The critical points are marked with arrows in Fig. 6 and the corresponding $\xi_{\parallel}$ are 54.0, 42.0, 25.8 and 12.6 nm for S-1, S-2, S-3 and S-4, respectively.

The vertical correlation length can also be determined in a simple way. According to Stearns (1992), the full width at half-maximum (FWHM) of the mth Bragg sheet is inversely proportional to $N_{\rm eff}$, the number of effectively correlated multilayer periods, *i.e.* FWHM $\simeq 2m\pi/N_{\rm eff}\Lambda$. We measured the FWHM of the first Bragg sheet for the four samples. The results and corresponding $N_{\rm eff}$ are shown in Fig. 7. At low q_y, $N_{\rm eff}$ of four samples are about 9–10, which are limited by the finite periodic number $N = 10$. At higher q_y, $N_{\rm eff}$ reduces with q_y. The multilayer grown at higher pressure has larger $N_{\rm eff}$, indicating more roughness replication. Salditt *et al.* (1994, 1996) showed that the FWHM follows the scaling law FWHM $\simeq q_y^z$, where z is the dynamic growth exponent. We performed a fit of FWHM $= a + bq_y^z$ to determine z, and the resulting z is 2.08, 2.05, 1.97 and 1.65 for S-1, S-2, S-3 and S-4, respectively. However, the error $\Delta z \simeq \pm 0.2$ is quite large because the power term is smaller than the constant term which is induced by the finite periodic number. The dynamic growth exponent z together with the roughness exponent α can identify the universality class of the growth process. Collating the obtained values with the known classes, we conclude that S-1, S-2 and S-3 belong to the Edwards–Wilkinson (EW) class ($\alpha = 0$, $z = 2$) and S-4 the Kardar–Parisi–Zhang (KPZ) class ($\alpha = 0.38$, $z = 1.58$) (Edwards & Wilkinson, 1982; Kardar *et al.*, 1986). The effects of sputter pressure on thin-film microstructure have been widely studied (Clemens, 1987; He *et al.*, 1991; Gómez *et al.*, 2002). Our results show that the morphology and the underlying growth process of W/Si multilayers change significantly at sputter pressures between 5 mTorr and 7 mTorr.

4. Summary and conclusions

In conclusion, we have demonstrated the integration method which can directly determine the average PSD function of a periodic multilayer from the X-ray scattering diagram measured in the out-of-plane geometry. In using this method, the measured scattering intensities are multiplied by an average roughness term $\exp(q_z^2\sigma_{\rm av}^2)$ and integrated along q_z in an interval which is decided by the thickness ratio. After these procedures, we can eliminate the contribution of cross-correlations to the integrated intensity without assuming any cross-correlation model and only the autocorrelations are reserved. Then the multilayer can be treated as a 'single interface' and the average PSD function can be obtained.

We have applied the integration method on the interface characterization of sputter-deposited W/Si multilayers grown at Ar pressures of 1, 3, 5 and 7 mTorr. The asymptotic behavior of the resulting PSD functions at high frequencies suggests a static roughness exponent of $\alpha = 0$ for the three 1–5 mTorr multilayers and $\alpha = 0.35$ for the 7 mTorr multilayer. The critical point of slope change in the log–log plot of the PSD functions indicates a lateral correlation length of 54.0, 42.0, 25.8 and 12.6 nm for the 1, 3, 5 and 7 mTorr multilayers, respectively. The FWHM of the Bragg sheets gives a measure of the vertical correlation length. The vertical correlation lengths of the four samples are limited by the finite period number at low frequencies and decay with the frequency. At high frequencies the sample grown at higher pressure has a larger vertical correlation length. The frequency-dependent behavior of the FWHM suggests a dynamic growth exponent $z = 2$ for the three 1–5 mTorr multilayers and $z = 1.65$ for the 7 mTorr multilayer. The static roughness exponent and dynamic growth exponent uniquely determine the universality class of the growth process. We have found that the samples grown at 1–5 mTorr agree with the EW class and the 7 mTorr sample agrees with the KPZ class.

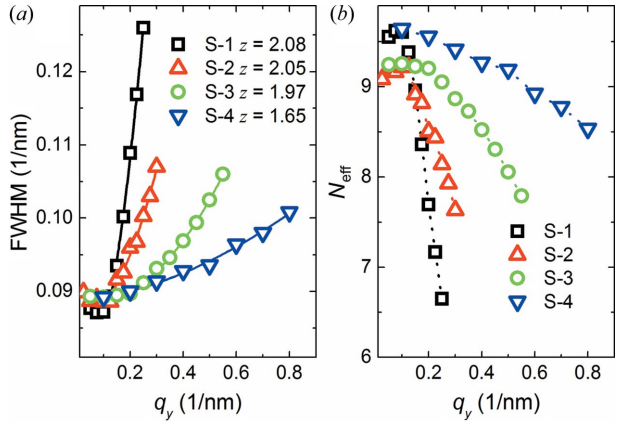

Figure 7
(*a*) FWHM (open symbols) of the first Bragg sheet *versus* q_y. Solid lines are the power-law fit. (*b*) Effectively correlated period number (open symbols) *versus* q_y. Dotted lines are guides for the eye only.

This work is supported by the National Natural Science Foundation of China (grant Nos. 10825521 and 10905042) and the 973 program (grant No. 2011CB922203).

References

Barabási, A.-L. & Stanley, H. E. (1995). *Fractal Concepts in Surface Growth.* Cambridge University Press.
Boer, D. K. G. de (1996). *Phys. Rev. B*, **53**, 6048–6064.
Clemens, B. M. (1987). *J. Appl. Phys.* **61**, 4525.
Edwards, S. F. & Wilkinson, D. R. (1982). *Proc. R. Soc. London A*, **381**, 17–31.
Gibaud, A. & Hazra, S. (2000). *Curr. Sci.* **78**, 1467–1477.
Gómez, M., Santamaria, J., Cyrille, M., Nelson, E., Krishnan, K. & Schuller, I. (2002). *Eur. Phys. J. B*, **30**, 17–23.
He, P., McGahan, W. A., Nafis, S., Woollam, J. A., Shan, Z. S., Liou, S. H., Sequeda, F., McDaniel, T. & Do, H. (1991). *J. Appl. Phys.* **70**, 6044–6046.
Holý, V. & Baumbach, T. (1994). *Phys. Rev. B*, **49**, 10668–10676.
Kardar, M., Parisi, G. & Zhang, Y. C. (1986). *Phys. Rev. Lett.* **56**, 889–892.
Kozhevnikov, I. V. & Pyatakhin, M. V. (2000). *J. X-ray Sci. Technol.* **8**, 253–275.
Krug, J. (1997). *Adv. Phys.* **46**, 139–282.
Müller-Buschbaum, P. (2003). *Anal. Bioanal. Chem.* **376**, 3–10.
Peverini, L., Ziegler, E., Bigault, T. & Kozhevnikov, I. (2007). *Phys. Rev. B*, **76**, 045411.

Renaud, G., Lazzari, R. & Leroy, F. (2009). *Surf. Sci. Rep.* **64**, 255–380.
Salditt, T., Lott, D., Metzger, T., Peisl, J., Vignaud, G., HOghOj, P., Schärpf, O., Hinze, P. & Lauer, R. (1996). *Phys. Rev. B*, **54**, 5860–5872.
Salditt, T., Metzger, T., Brandt, C., Klemradt, U. & Peisl, J. (1995). *Phys. Rev. B*, **51**, 5617–5627.
Salditt, T., Metzger, T. H. & Peisl, J. (1994). *Phys. Rev. Lett.* **73**, 2228–2231.
Siffalovic, P., Jergel, M., Chitu, L., Majkova, E., Matko, I., Luby, S., Timmann, A., Roth, S. V., Keckes, J., Maier, G. A., Hembd, A., Hertlein, F. & Wiesmann, J. (2010*a*). *J. Appl. Cryst.* **43**, 1431–1439.
Siffalovic, P., Majkova, E., Chitu, L., Jergel, M., Luby, S., Keckes, J., Maier, G., Timmann, A., Roth, S. V., Tsuru, T., Harada, T., Yamamoto, M. & Heinzmann, U. (2010*b*). *Vacuum*, **84**, 19–25.
Sinha, S. K. (1994). *J. Phys. III Fr.* **4**, 1543–1557.
Sinha, S. K., Sirota, E. B., Garoff, S. & Stanley, H. B. (1988). *Phys. Rev. B*, **38**, 2297–2311.
Spizzo, F., Ferrero, C., Mazuelas, A., Albertini, F., Casoli, F., Nasi, L., Ronconi, F. & Metzger, T. H. (2009). *J. Appl. Phys.* **105**, 123533.
Stearns, D. G. (1992). *J. Appl. Phys.* **71**, 4286.
Underwood, J. H. & Barbee, T. W. (1981). *Appl. Opt.* **20**, 3027–3034.
Wormington, M., Panaccione, C., Matney, K. M. & Bowen, D. K. (1999). *Philos. Trans. R. Soc. London A*, **357**, 2827–2848.